ICEMG 2023-XXXXX

Dynamic Load Emulation for Evaluating EVs Machines Based on Sliding Mode Control

Mohammadreza Adib[1], Abolfazl Vahedi[1]

[1]Iran University of Science and Technology, Tehran, Iran
Mohammadreza_adib@elec.iust.ac.ir, aVahedi@iust.ac.ir

Abstract

Dynamometers are widely used for electric machines and their drive systems assessment, reducing prototyping time for many applications, such as Electric Vehicles machines. Having the same mechanical topology allows changing the control algorithm to significantly improve the overall functionality. Hence, this paper proposes dynamic load emulation by utilizing sliding mode control. The proposed method is characterized by its simplicity, robustness, and low computational effort. A proper sliding manifold is designed in which the sliding manifold contains the desired dynamic. The control signal is derived from that, which consists of two parts; the first part is based on the dynamics of the system, and the second part is a switching function, responsible for the rejection of disturbances. Thus, dynamic load emulation (DLE) can be attained with a fast and precise response to various linear and nonlinear loads based on the mathematical model of the desired load. The desired model of mechanical load provides the speed reference to achieve the desired dynamic by forcing the shaft to rotate at a specific speed. The approach has been validated using a linear and a nonlinear load. The perfect tracking of the reference has shown that emulation still can be carried out despite uncertainty in the model and disturbances.

Keywords: dynamic load emulation; dynamometer; electric machines test bench; mechanical load emulation; sliding mode control.

Introduction

Dynamometers must be able to resemble the actual mechanical load conditions for the motor under test (MUT) so that the characteristics of the electric machines can be evaluated in real-world situations, such as those dynamic behaviors that present on the road. It is usually complicated, potentially time-consuming, and even impossible to replicate the real situation within a laboratory environment. Also, it is more efficient to use dynamometers instead of building a complete setup. It has been found that passive dynamometers (such as eddy current) are primarily used to simulate and provide constant loads, which are known as static tests and can provide information about efficiency, temperature, torque-speed characteristics, vibration, and so on [1]–[4]. A rapid prototyping technique, known as the dynamic emulation of mechanical loads, was created to assess the performance of drives in mechanisms in comparison to the traditional approach. It is an interesting new tool for the design of algorithms for controlling variable speed and torque in mechatronics. It enables the development of controllers for diverse components without the requirement of a prototype, as well as multiple testing options. It allows for the examination of varying inertia and highly nonlinear dynamics [4]. Meanwhile, with the rapid growth in demand for electric vehicles (EVs), it is imperative to evaluate traction motors which are widely used in EVs, their drive system, and transmission in a dynamic situation [5]. It is recommended that facilities should be evaluated under dynamic conditions, such as accelerating and braking, that a machine can be encountered during transient periods. Various methods have been proposed for conducting research on hybrid electric vehicles (HEVs) and EVs [3]. Insights into the vehicle's functionality can be generated by testing the vehicle's chassis on a dynamometer [6]. The chassis dynamometers require a complete setup, while alternative dynamometers are available that can be coupled directly to the shaft of MUT, as shown in Figure 1; therefore, only the motor and drive system can be properly assessed during the early stages of development. A mathematical model as shown in Figure 1(b) can replace the entire actual mechanical load shown in Figure 1(a) and generate a reference for the load machine to act as the mechanical load. Hardware-in-the-loop simulations are also popular, as this method can significantly reduce testing time and expenses. Verification can be conducted using hardware-in-the-loop test procedures during the preliminary phases of development. Using this method, the control hardware interfaces with a real-time simulator that has models of the system [5].

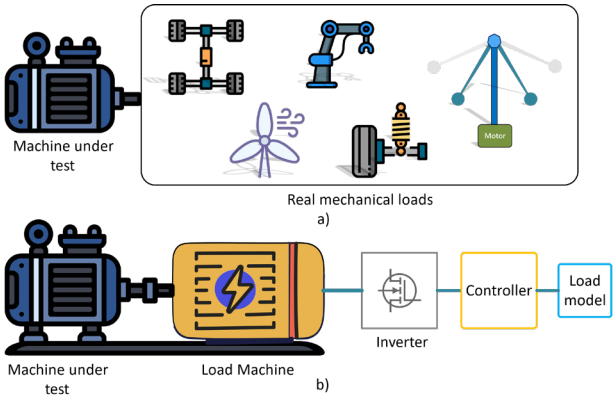

Figure 1. Replacing actual load with load machine. (a): MUT is in direct contact with actual loads. (b): Load machine emulates actual load behavior based on the desired model.

Several software- and hardware-related equipment make up the advanced electric machine test bench. Within the software part, the model of desired mechanical load model, data collected from sensors, and control algorithm exist. Hardware contains two coupled machines, a base frame, sensors, etc. Considering that the hardware topology is almost identical, enhancing the control strategy at the software stage can have a significant impact on the overall functionality of the same test bed. Hence, having a control algorithm that can be robust enough is

vital. Existing parameter variations, disturbances, model uncertainties, and structural uncertainties are the reason for utilizing a robust control algorithm to have precise trajectory tracking [7], [8]. As the mechanical structures in the dynamometers are the same, updating the control section that is robust and simple to implement is paramount to have a more accurate emulation. However, the mechanical coupling can affect the control algorithm's performance. For example, the backlash effect and flexible shaft cause difficulties and stability issues. Thus, in [9], to address the problem of poor stability and accuracy during the load emulation of a rigid-flexible shaft with a compound correction compensation for the control method is proposed. A variety of approaches to dynamic load emulation (DLE) has been presented in recent research. The inverse mechanical dynamic (IMD) used to be applied in many studies such as [1], [2], [10]–[12] due to its simplicity. The IMD provides a torque reference without dynamic load emulation and does not guarantee that the desired dynamics will be preserved. The main demerit of the IMD approach is the noise of its output. The derivative terms in the equations lead to noise, which may cause instability [13], [14]; a filter can be used to the produced noise to alleviate, but it lowers the speed of response. Taking advantage of a system transient response, [14] proposes a compensator. Through the analysis of transient system step response from experimental testing data, it is possible to fully design this compensator based on parametric system identification. Some references, such as [12], [15], [16], utilized a proportional-integral (PI) controller to imitate the mechanical load behavior. By changing the load model, the PI-based controllers need to tune every time in order to keep a good performance. Furthermore, in [17], an induction motor was able to replicate an internal combustion engine system thanks to an auto-tuned PI speed controller. To imitate the dynamics of a wind turbine drivetrain in a wider control bandwidth than a typical PI control, a PID speed controller and a hysteresis current control were designed in [18]. Power electronics-controlled machines are dynamically fast, so they are able to emulate conventional mechanical systems more easily than conventional mechanical systems. Despite this fact, the designed controller is limited to a specific system and cannot be adapted to applications requiring faster dynamic response time. A number of approaches are presented in the literature to address these issues, including Model Predictive Control (MPC) approach that can handle the requirement for high performance, input and output constraints, and optimal control signals. The authors of [19] presented a dynamometer based on two-degree-of-freedom (2-DOF) feedforward MPC has been presented for combustion engines. Conventional state feedback and 2-DOF flatness-based feedforward are discussed, then the results of the proposed 2-DOF MPFFC show improvement compared to the previously discussed methods. In general, the MPC could provide optimal signals within the system constraints; however, there are some drawbacks to using it. The MPC is dependent on the model and parameters; besides, due to solving a cost function in every time step, the computational effort enforces the utilization of advanced hardware. In [20], a new DLE method has been proposed for emulating mechanical loads based on a mathematical model and uses a compensator with a speed-tracking controller. The given results of the paper illustrate a very good representation of the desired mechanical linear and nonlinear load behavior that can be achieved under parameter variation.

Dynamic Load Emulation principle

Real-world systems are typically nonlinear, and nonlinear systems are neither homogeneous nor follow the principle of superposition. In addition, uncertainty and unmodeled dynamic, can cause the controller to suffer serious problems [7]. In EVs application, emulating various kinds of loads is needed to imitate the real situation for the motor and the drive system associated with it. Considering the uncertainties and parameter variations in dynamometer systems and the nonlinear nature of the desired load, this research presents and evaluates the sliding mode control for dynamic load emulation to solve these problems. The simplified system is illustrated in Figure 2. It is the permanent magnet type machine that is widely used in EV applications due to its high efficiency, high power density, and other beneficial characteristics [20]–[23]. In dynamic load emulation, the main objective is to force the actual speed to reach the emulated speed (W_{em}) produced by the load model during the transients. The emulated speed is the speed that both machines, which are mechanically connected, should follow as a reference to the desired dynamic that can be emulated. In this concept, the model of the desired load is available, and the electromagnetic torque produced by the MUT can be measured or estimated.

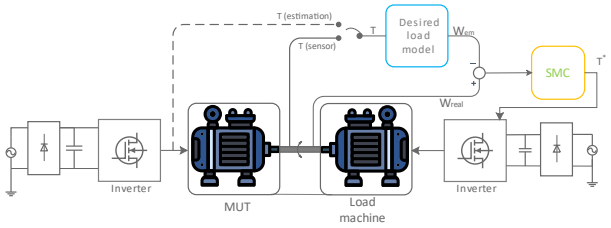

Figure 2. Diagram of system with MUT and Load machine.

According to Figure 3, The mechanical dynamic equation of the actual system is:

$$T_m + T_e = J\dot{\omega}_r + B\omega_r \quad (1)$$

Where T_m and T_e are the load machine and drive machine torque, respectively; ω_r is the shaft speed. J and B are the total inertia and viscous coefficient of both machines. With $T_L = 0$, the MUT will experience only the inertia of the motor under test, J_1, while the desired inertia is J_{em}.

To put it in another way, the transfer function (in which 's' is the Laplace transform operator) of the motor (e.g., electric vehicle) in a real situation is:

$$G_r(s) = \frac{\omega_r(s)}{T_m(s)} \quad (2)$$

Moreover, the transfer function of the motor in the desired situation, like a road, can be defined as:

$$G_{em}(s) = \frac{\omega_{em}(s)}{T_m(s) - T_e(s)} \quad (3)$$

To assure that the desired behavior is implying on the MUT, these two transfer functions (equations 2 and 3)

should become ideally the same; hence, T_e is needed to exert an additional torque on the shaft to control the acceleration or deceleration rate of the whole system; thus, the desired dynamic could be met when the real speed tracks perfectly the emulated speed that is generated by the desired load model.

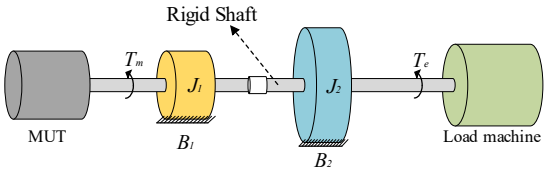

Figure 3. Simplified representation of mechanical coupling.

Control algorithm

The sliding mode controller (SMC) is of interest since the nonlinear nature of the controller is suitable for use with systems that contain nonlinear dynamics [7], [24]–[26]. Many existing approaches that are reviewed in the first section are not fast and robust or require tuning the parameters in order to have better performance. Hence, here sliding mode control is explained based on the aforementioned principle of dynamic load emulation. The first step in designing an SMC is to create an intermediate variable S (sliding manifold) such that $\dot{s}$ contains u (input control), and while S goes to zero, the error goes to zero; thus, generally, a candidate could be as (4). For a second-order system, the value of n is two, so the sliding manifold by choosing n = 2 in equation (4) can be driven as (5). By rearranging equation (5), it can be easily shown that the error goes to zero when the sliding variable goes to zero. Meanwhile, the derivative of the sliding variable contains $\ddot{\theta}$ in which from the state equation of the system, the input control signal appears in the sliding variable.

$$s = \left(\frac{d}{dt} + \lambda\right)^{n-1} e \tag{4}$$

$$s = \dot{e} + \lambda e \tag{5}$$

Error and the derivative of error are defined as (6):

$$e(t) = \theta(t) - \theta_{\mathrm{d}}(t),$$

$$\dot{e}(t) = \dot{\theta}(t) - \dot{\theta}_{\mathrm{d}}(t) \tag{6}$$

θ is the rotor angle, θ_{d} the desired angle produced by the load model in order to achieve the desired dynamic, and λ is a positive constant. The value of λ can be set by trial and error. By choosing λ large enough, the controller sees a larger error, and consequently, the response would be faster but too high value for it leads to fast changes in response to minor errors; in this application, the value of λ is considered to be roughly 20. The second step is to design the control signal, which consists of two parts, the first part is designed based on the ideal mechanism that is obtained from the derivative of the sliding manifold (u1), and the second part is the switching function of the sliding manifold (u2). Figure 4 shows different starting points as the initial condition. The first part of the control signal, which is defined as u1, forces the state variables to reach the sliding manifold in which it has the desired dynamics. Meanwhile, the second part of the control signal, which is defined as u_2, keeps the state variable within the vicinity of the sliding manifold as the actual system does not entirely match the ideal one. In fact, because of uncertainties and disturbances, some error is produced and makes a non-zero value for S, resulting in the switching part acting in a negative direction to suppress the disturbances and uncertainties.

$$u_1(t) = \frac{1}{b}\left[-\hat{f} - \lambda\dot{e} + \ddot{e}_d\right],$$

$$u_2(t) = -\eta \times \mathrm{sign}(S),$$

$$U = u_1 + u_2 \tag{7}$$

In which sign(s) is:

$$sign\,(S) = \begin{cases} 1 & S > 0 \\ 0 & S = 0 \\ -1 & S < 0 \end{cases} \tag{8}$$

If the dynamic of system is assumed to be $\ddot{x} = f(x) + b(x)u$, $\hat{f}$ is an estimation of the system, b is the input vector, and η can be supposed as the upper band of uncertainties which will explain in the following sections.

According to Figure 4, if the state variables of the system approach the sliding manifold, S will approach zero. When S becomes negative, the value of sign(s) will be +1, so the amplitude of the switching part will be -η. Also, as S becomes positive, the amplitude of the switching part will be +η instantly which means high-frequency changes in the control signal. As a consequence, the chattering problem during the sliding phase stimulates the higher-order emergence of unmodeled dynamics. Furthermore, since the switching frequency of power electronics devices has an upper limit, it is not feasible to support the changes in the control signals. In this paper as an effective way to address the chattering issue, a saturation-type function for the switching function is used.

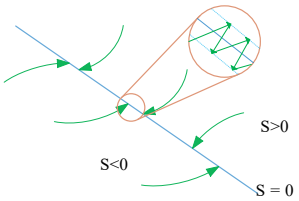

Figure 4. Sliding manifold and chattering phenomena

Lyapunov stability analysis

By supposing the Lyapunov function candidate as (9), and according to the Lyapunov stability criterion, the Lyapunov function must be positive, and the derivative of it must be negative for a considered system to stay stable. Based on (9), the assumed Lyapunov function is always positive, and the derivative of it must be proved to be negative. By supposing the derivative of the Lyapunov function is negative, such as (10), and reforming the equation to achieve equation (11), which is called the sliding condition, two cases can be defined as (12) and (13).

$$V(S) = \frac{1}{2}S^2 \tag{9}$$

$$\dot{V}(S) = \frac{1}{2}\frac{d}{dt}(S^2) = S\dot{S} < 0 \tag{10}$$

$$S\dot{S} < -\eta|S| < 0 \text{ and } \eta > 0 \tag{11}$$

$$s > 0 \;\Rightarrow\; S\dot{S} < -\eta S \Rightarrow \dot{S} < -\eta \tag{12}$$

$$s < 0 \;\Rightarrow\; S\dot{S} < \eta S \Rightarrow \dot{S} > \eta \tag{13}$$

If S is positive, according to (12), both S on each side of the equation cancels out, and the derivative becomes negative. In this case, the derivative of Lyapunov, which

is (10), becomes negative. When S becomes negative, the derivative would be positive, and again the equation (10) becomes negative; in both cases, the sliding manifold is absorbing, regardless of where the initial states are located. As beforementioned, the η should be large enough to cover the uncertainties, so the state variables stay in the vicinity of the sliding manifold; besides, it can be easily shown that reaching occurs in finite time.

Controller design

In this section, one linear and one load are considered for design.

A. Linear model

For evaluating the controller's response, a linear load is described by (14) and is presented as the desired load model in Figure 2. For a linear load that is described as (14), J_{em} and B_{em} are the desired inertia and viscous friction, respectively.

$$G_{em} = \frac{1}{J_{em}\ddot{\theta} + B_{em}\dot{\theta}} \tag{14}$$

As previously explained, an intermediate sliding manifold can be considered as:

$$s(t) = \dot{e}(t) + \lambda e(t) \tag{15}$$

In which $e(t)$ and $\dot{e}(t)$ are as below

$$e(t) = \theta(t) - \theta_{\mathrm{d}}(t)\,,$$
$$\dot{e}(t) = \dot{\theta}(t) - \dot{\theta}_{\mathrm{d}}(t) \tag{16}$$

The derivative of the sliding variable contains the input signal which is T_L in this concept. Meanwhile, equation (14) has the $\ddot{\theta}$ term. By rearranging equation (14) and putting the reformed equation in the derivative of sliding manifold (17), signal control can be obtained.

$$\dot{s}(t) = \dot{e}(t) + \ddot{e}(t)\dot{e}(t) + \ddot{\theta}(t) - \ddot{\theta}_{\mathrm{d}}(t) \tag{17}$$

$$T_e + T_l = J\ddot{\theta} + B\dot{\theta} \Rightarrow \ddot{\theta} = \frac{1}{J}\left(T_e + T_l - B\dot{\theta}\right) \tag{18}$$

$$\dot{s} = \dot{e}(t) + \left(T_e + T_l - B\dot{\theta}\right)/J - \ddot{\theta}_{\mathrm{d}}(t) = 0 \tag{19}$$

$$T_l = J\ddot{\theta}_d + B\dot{\theta} - Te - J\lambda\left(\dot{\theta} - \dot{\theta}_d\right) \tag{20}$$

The first part of the control signal is expressed by equation (20). By subtracting the switching part, the complete signal control will be:

$$U = J\ddot{\theta}_d + B\dot{\theta} - Te - J\lambda\left(\dot{\theta} - \dot{\theta}_d\right) - \eta \times \mathrm{Sgn}(S) \tag{21}$$

B. Nonlinear model

To assess the functionality of controller for nonlinear loads, watt governor model is used in many references. Figure 5 illustrates a simplified watt governor load; applying torque to the shaft and increasing the speed causes the flying balls to go up; hence, the inertia and viscous friction coefficients will vary and exhibit nonlinear behavior. Watt governor model equations can be expressed as follow:

$$\dot{x}_1 = -\frac{B_{\mathrm{em}} + 2m\ell^2 x_2 \sin(2x_3)}{J_{\mathrm{em}} + 2m\ell^2 \sin^2(x_3)} x_1 + \frac{1}{J_{\mathrm{em}} + 2m\ell^2 \sin^2(x_3)} T_e,$$

$$\dot{x}_2 = -\frac{B_o}{m\ell^2} x_2 + \frac{1}{2} x_1^2 \sin(2x_3) - \frac{g}{\ell} \sin(x_3),$$

$$\dot{x}_3 = x_2 \tag{22}$$

here J_{em} and B_{em} are defined as:

$$J_{\mathrm{ef}} = J_{\mathrm{em}} + 2m\ell^2 \sin^2\theta \tag{23}$$
$$B_{\mathrm{ef}} = B_{\mathrm{em}} + 2m\ell^2\dot{\theta}\sin(2\theta) \tag{24}$$

And the state vector is $x = \left[\omega, \dot{\theta}, \theta\right]^T$.

Similar to the previous procedure for a linear load, the control signal for a watt governor load based on equations (22) - (24) can be calculated as:

$$U = B_{ef}\dot{x}_1 + J_{ef}\ddot{x}_1^{\,*} - T_e - \lambda J_{ef}(\dot{x}_1 - \dot{x}_1^*) - \eta \times \mathrm{Sgn}(S) \tag{25}$$

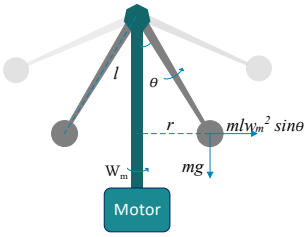

Figure 5. Watt governor model

Simulation results

In this section, the simulation results of two loads are provided. The lumped inertia of both machines is 0.004 kg.m^2, and the viscous friction is 0.008 N.m.s. First, a linear load with J_{em} = 0.002 kg.m^2 and B_{em} = 0.01 N.m.s are set to show that the dynamometer can emulate the lower dynamics of the total system. The lower the inertia, the more challenging it is to track the reference, because lower inertia leads to higher dynamics and faster changes in the reference. In order to aggravate the situation and validate the controller robustness in the presence of disturbances, an arbitrary disturbance is added to the system in t = 0.15 seconds. Figure 6(a) shows step changes in MUT's speed reference and the load machine helps the MUT to accelerate in step changes in order to see lower inertia than lumped inertia of both machines. To illustrate the reaching phase and sliding phases, the initial value of the emulated speed is set at about 50 rpm. Consequently, at the beginning, the difference between the real speed and emulated speed is large. During the reaching phase, the value of the sliding variable is large, resulting in a larger control signal as shown in Figure 6(b). In the magnified section of Figure 6(a), the error between real speed and desired speed dramatically decreases. After applying disturbance, Figure 6(a) shows that the real speed is kept virtually close to the desired speed.

Figure 6(b) shows the disturbance and control signal input simultaneously to exhibit the rejection of the injected disturbance. While disturbance leads to higher error in speed tracking, the second part of the control input compensates for the effects of it and suppresses the disturbances. As the system distances from the desired reference, the value of S becomes larger, leading to higher u_2 in the control input. This part will be subtracted from u_1, and the actual system does not see the disturbances. The emulation is repeated for J_{em} = 0.015 and B_{em} = 0.02 to show the capability of emulating different J and B, as shown in Figure 7.

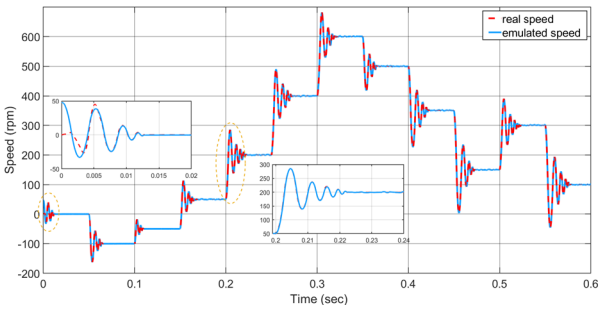

(a)

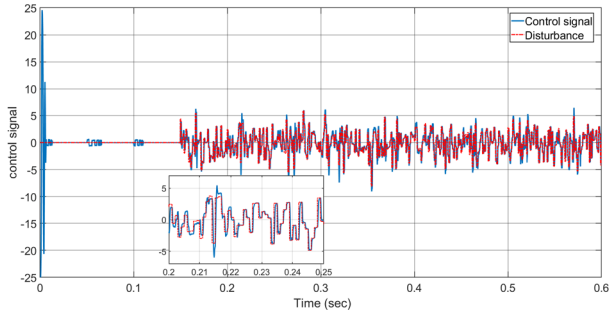

(b)

Figure 6. Emulating linear load with J_{em}=0.002 and B_{em}=0.01. (a) precise reference tracking of step changes; (b) control signal and disturbance.

By increasing the inertia of the system, the dynamic of the system will become slower. Obviously, for a higher value of inertia, more torque will be needed in order to produce a higher value of torque. Since the dynamics for lower inertia is faster than the higher value of inertia for loads, if the controller can replicate the desired load behavior, it will be capable of emulating slower dynamics. In conclusion, the dynamometer based on SMC can emulate different inertia and viscous friction and reject the disturbances. Results show fast and accurate mechanical load behavior emulation for the motor under test.

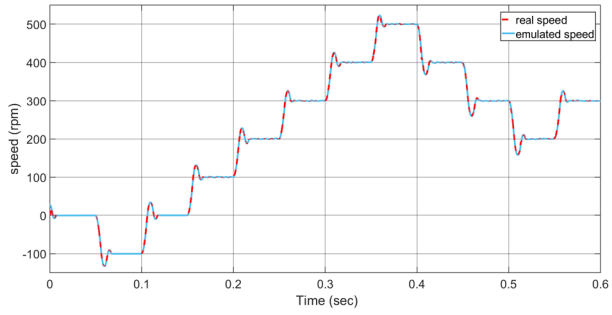

Figure 7. Emulating linear load with J_{em}=0.015 and B_{em}=0.02.

Additionally, a watt governor model is placed in the load model block as a representation of a nonlinear load. Figure 8(a) shows the step changes in MUT's speed command. The most nonlinearity behavior occurs while balls in the governor go up as shown in Figure 8(b); hence, inertia and viscous friction that the MUT sees will change as a function of the degree of balls as presented in equations (22). In Figure 8(a), it can be seen that the emulated speed changes in a way that the motor under test experiences the situation as if it was connected to a real watt-governor. This interval is magnified in Figure 8(a) to show the accuracy of the dynamic load emulation. As the most nonlinearity behavior of the desired load occurs in this interval, when the controller can follow the reference in this interval, it will be able to track the trajectory of other changes. Besides, like the linear load, an arbitrary disturbance is injected into the system in t = 0.15s to show the robustness of the controller.

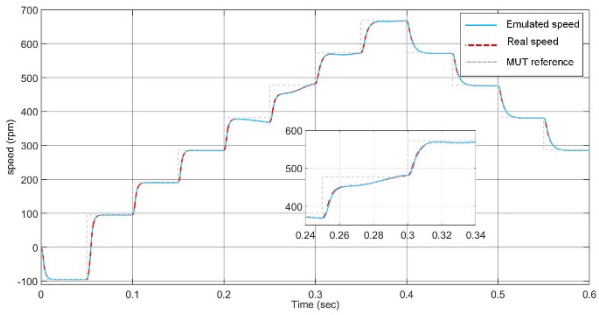

(a)

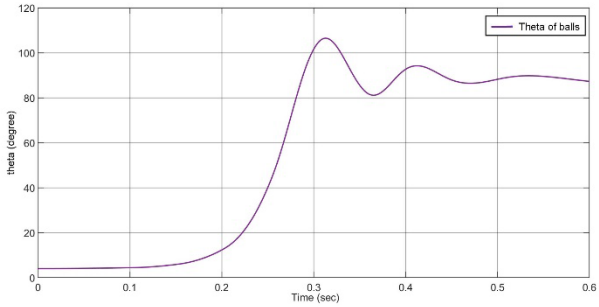

(b)

Figure 8. Emulating nonlinear load with J_{ef}=0.008 and B_{ef}=0.01. (a) step reference; (b) the degree of balls.

Conclusions

In many fields, such as electric vehicle machines, dynamometers are widely used for the assessment of electric machines and their drive systems. This reduces the time required for prototyping. Dynamic load emulation can be attained when the shaft rotates at the given speed by the desired load model. In this paper, dynamic load emulation in different situations has been achieved. The given results show that the load machine can mimic the behavior of the desired load model by forcing the shaft to rotate at a specific speed. Hence, the accuracy of the approach can be evaluated by the error between the emulated speed (reference speed) and the actual speed. The proposed method is characterized by its simplicity, robustness, and low computational. Results show the robustness of the approach by rejecting the injected disturbance. Also, varying the load parameters, without changing the controller shows the robustness of the approach under parameter variation and other types of uncertainties for both linear and nonlinear loads.

References

[1] P. Sandholdt, E. Ritchie, J. K. Pedersen, and R. E. Betz, "Dynamometer performing dynamical emulation of loads with non-linear friction," in *IEEE International Symposium on Industrial Electronics*, 1996, vol. 2, pp. 873–878. doi: 10.1109/isie.1996.551058.

[2] E. R. Collins and Y. Huang, "A Programmable Dynamometer for Testing Rotating Machinery Using a Three-Phase Induction Machine," *IEEE Transactions on Energy Conversion*, vol. 9, no. 3, pp. 521–527, 1994, doi: 10.1109/60.326471.

[3] T. Akiyama, M. Kobayashi, Y. Sawada, and M. Nomura, “Control of Standard Engine Test Bench System for Dynamic Road Load Tests,” in *2006 SICE-ICASE International Joint Conference*, 2006, pp. 1566–1569. doi: 10.1109/SICE.2006.315447.

[4] W.-L. Li, J.-J. Wang, X.-K. Zhang, and P. Yi, “A novel road dynamic simulation approach for vehicle driveline experiments,” *Discrete & Continuous Dynamical Systems - S*, vol. 12, no. 4–5, pp. 1035–1052, 2019, doi: 10.3934/dcdss.2019071.

[5] N. Sharma, B. Jiang, A. Rodionov, and Y. Liu, “A Mechanical-Hardware-in-the-Loop Test Bench for Verification of Multi-Motor Drivetrain Systems,” *IEEE Transactions on Transportation Electrification*, pp. 1–1, 2022, doi: 10.1109/TTE.2022.3191411.

[6] A. von Jouanne *et al.*, “Electric Vehicle (EV) Chassis Dynamometer Testing,” in *2020 IEEE Energy Conversion Congress and Exposition (ECCE)*, Oct. 2020, pp. 897–904. doi: 10.1109/ECCE44975.2020.9236288.

[7] Jean-Jacques E. Slotine and Weiping Li, *Applied Nonlinear Control*. Prentice Hall, 1991.

[8] L. Hou, J. Ma, and W. Wang, “Sliding Mode Predictive Current Control of Permanent Magnet Synchronous Motor With Cascaded Variable Rate Sliding Mode Speed Controller,” *IEEE Access*, vol. 10, 2022, doi: 10.1109/ACCESS.2022.3161629.

[9] H. Li, Z. Zhao, and P. Tang, “Load Emulation Compensation Control of a Test Bench Based on Rigid-Flexible Coupling Transmission for a Vehicle Electric Drive System,” *IEEE Trans Instrum Meas*, vol. 71, pp. 1–16, 2022, doi: 10.1109/TIM.2022.3204095.

[10] K. Kyslan and F. Ďurovský, “Dynamic Emulation of Mechanical Loads - An Approach Based on Industrial Drives’ Features,” *Automatika – Journal for Control, Measurement, Electronics, Computing and Communications*, vol. 54, no. 3, Sep. 2013, doi: 10.7305/automatika.54-3.184.

[11] W. Wang, W. Zhang, and X. Li, “Inertia electrical emulation and angular acceleration estimation for transmission test rig,” *Dongnan Daxue Xuebao (Ziran Kexue Ban)/Journal of Southeast University (Natural Science Edition)*, vol. 42, no. 1, 2012, doi: 10.3969/j.issn.1001-0505.2012.01.012.

[12] M. Rodič, K. Jezernik, and M. Trlep, “Control design in mechatronic systems using dynamic emulation of mechanical loads,” in *IEEE International Symposium on Industrial Electronics*, 2005, vol. IV. doi: 10.1109/ISIE.2005.1529177.

[13] Z. H. Akpolat, “Dynamic emulation of mechanical loads using a vector-controlled induction motor-generator set,” *IEEE Transactions on Industrial Electronics*, vol. 46, no. 2, pp. 370–379, 1999, doi: 10.1109/41.753776.

[14] C. Gan, R. Todd, and J. M. Apsley, “Drive system dynamics compensator for a mechanical system emulator,” *IEEE Transactions on Industrial Electronics*, vol. 62, no. 1, 2015, doi: 10.1109/TIE.2014.2327581.

[15] K. Kyslan, M. Rodič, Ľ. Suchý, Ž. Ferková, and F. Ďurovský, “Industrial controller-based dynamometer with dynamic emulation of mechanical loads,” *Electrical Engineering*, vol. 99, no. 4, pp. 1245–1254, Dec. 2017, doi: 10.1007/s00202-017-0626-z.

[16] M. Rodič, K. Jezernik, and M. Trlep, “Dynamic emulation of mechanical loads: An advanced approach,” *IEE Proceedings: Electric Power Applications*, vol. 153, no. 2, 2006, doi: 10.1049/ip-epa:20050063.

[17] E. J. Thomas and P. W. Sauer, “Engine-simulation control of an induction motor,” in *Proceedings - Electrical Insulation Conference and Electrical Manufacturing and Coil Winding Conference, EEIC 1999*, 1999. doi: 10.1109/EEIC.1999.826275.

[18] L. A. C. Lopes, J. Lhuilier, A. Mukherjee, and M. F. Khokhar, “A wind turbine emulator that represents the dynamics of the wind turbine rotor and drive train,” in *PESC Record - IEEE Annual Power Electronics Specialists Conference*, 2005, vol. 2005. doi: 10.1109/PESC.2005.1581921.

[19] D. Erdogan, S. Jakubek, C. Mayr, and C. Hametner, “Model Predictive Feedforward Control for High-Dynamic Speed Control of Combustion Engine Test Beds,” *IEEE Open Journal of Industry Applications*, vol. 2, 2021, doi: 10.1109/ojia.2021.3073884.

[20] C. M. R. de Oliveira, M. L. de Aguiar, A. G. de Castro, P. R. U. Guazzelli, W. C. de Andrade Pereira, and J. R. B. de Almeida Monteiro, “High-Accuracy Dynamic Load Emulation Method for Electrical Drives,” *IEEE Transactions on Industrial Electronics*, vol. 67, no. 9, pp. 7239–7249, Sep. 2020, doi: 10.1109/TIE.2019.2942566.

[21] Y. Zhang, W. P. Cao, and J. Morrow, “Interior permanent magnet motor parameter and torque ripple analysis for EV traction,” in *2015 IEEE International Conference on Applied Superconductivity and Electromagnetic Devices (ASEMD)*, Nov. 2015, pp. 386–387. doi: 10.1109/ASEMD.2015.7453625.

[22] P. Pillay and R. Krishnan, “Application characteristics of permanent magnet synchronous and brushless DC motors for servo drives,” *IEEE Trans Ind Appl*, vol. 27, no. 5, pp. 986–996, 1991, doi: 10.1109/28.90357.

[23] P. B. Reddy, A. M. El-Refaie, K.-K. Huh, J. K. Tangudu, and T. M. Jahns, “Comparison of Interior and Surface PM Machines Equipped With Fractional-Slot Concentrated Windings for Hybrid Traction Applications,” *IEEE Transactions on Energy Conversion*, vol. 27, no. 3, pp. 593–602, Sep. 2012, doi: 10.1109/TEC.2012.2195316.

[24] J. de Santiago *et al.*, “Electrical Motor Drivelines in Commercial All-Electric Vehicles: A Review,” *IEEE Trans Veh Technol*, vol. 61, no. 2, pp. 475–484, Feb. 2012, doi: 10.1109/TVT.2011.2177873.

[25] Y. Niu, D. W C Ho, and J. Lam, “Robust integral sliding mode control for uncertain stochastic systems with time-varying delay,” *Automatica*, vol. 41, no. 5, pp. 873–880, May 2005, doi: 10.1016/j.automatica.2004.11.035.

[26] V. Utkin and Jingxin Shi, “Integral sliding mode in systems operating under uncertainty conditions,” in *Proceedings of 35th IEEE Conference on Decision and Control*, pp. 4591–4596. doi: 10.1109/CDC.1996.577594.